ACS Chemical Biology

Letter

Photocontrol of the Hv1 proton channel

Andreas Rennhack, Elena Grahn, Benjamin U. Kaupp, and Thomas K Berger

ACS Chem. Biol., **Just Accepted Manuscript** • DOI: 10.1021/acschembio.7b00523 • Publication Date (Web): 12 Oct 2017

ACS Publications

ACS Chemical Biology is published by the American Chemical Society. 1155 Sixteenth Street N.W., Washington, DC 20036

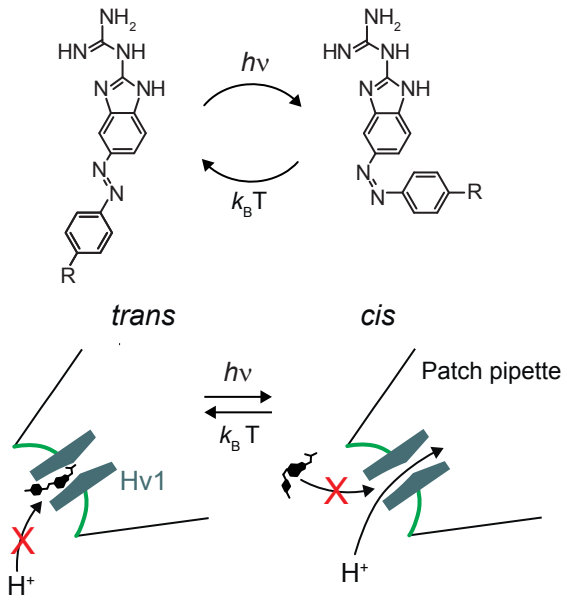
NH2
HN
NH
N
NH
N
N
R
hν
kBT
trans
cis
Patch pipette
Hv1
H+

Photocontrol of the Hv1 proton channel

Andreas Rennhack*, Elena Grahn*, U. Benjamin Kaupp, Thomas K. Berger

Department of Molecular Sensory Systems, Research Center Caesar, Ludwig-Erhard-Allee 2, 53175 Bonn, Germany

Abstract

The voltage-gated proton channel Hv1 is expressed in various human cell types, including macrophages, epithelial cells, and sperm. Hv1 opening leads to proton efflux that alkalizes the cytosol. Here, we describe light-activated Hv1 inhibitors (photoswitches) that allow controlling its activity with high spatiotemporal precision. The photoswitches comprise a light-sensitive azobenzene moiety and 2-guanidinobenzimidazole (2GBI), a known Hv1 inhibitor. In the dark, photoGBI inhibits heterologously expressed Hv1 channels. Blue light, which isomerizes the azobenzene group from *trans* to *cis* conformation, releases inhibition. We demonstrate photocontrol of native proton currents in human macrophages and sperm using photoGBI, underlining their use as valuable optochemical tools to study the function of Hv1 channels.

*equal contribution

Corresponding author: Thomas K. Berger, thomas.berger@caesar.de

Molecules that can be switched by light between active and inactive forms are powerful tools to control cellular processes with high spatial and temporal precision. One class of particularly useful photoswitches is based on an azobenzene scaffold attached to an effector molecule that can activate or inhibit target proteins, e.g. ion channels or receptors [1, 2, 3]. Azobenzenes exist as *trans* and *cis* isomers; irradiation by UV light converts *trans* to *cis*, and blue or green light converts *cis* back to *trans*. A change in azobenzene conformation alters the affinity or accessibility of a covalently attached activator or inhibitor to its target. A favorable property of azobenzenes is that they are photostable and resist photobleaching during long or repetitive light stimulation. Furthermore, azobenzenes can be chemically modified and, thereby, their substrate specificity, excitation wavelength, isomer stability, or solubility can be tuned. Azobenzene-based photoswitches have been successfully developed to control voltage- and ligand-gated ion channels [4, 5, 6, 7, 8, 9, 10]. More recently, the approach has been extended to control signal transduction pathways and enzymatic reactions [11, 12, 13, 14].

Here we develop a light-controlled, azobenzene-based inhibitor of the voltage-gated proton channel Hv1, which mediates proton extrusion and serves important physiological roles in various cells. In macrophages, Hv1 regulates the intracellular pH (pH_i) during production of reactive oxygen species [15, 16, 17]. In B lymphocytes, Hv1 regulates B-cell-receptor signaling [18]. In lung epithelial cells, Hv1 regulates the pH of the airway surface mucosa [19]. In several types of cancer, Hv1 is overexpressed, but its physiological role is unclear [20, 21]. Finally, in human sperm, Hv1 has been suggested to play a role in capacitation that enables egg fertilization [22]. A common denominator of these various cells is that changes in pH_i or extracellular pH (pH_o) are important ingredients of signaling. However, other proton transport pathways, like sodium-proton exchangers, also participate in pH regulation, and the functional consequences of Hv1 activation under physiological conditions have been difficult to investigate (see for example [23] for discussion). A light-controlled Hv1 inhibitor might facilitate further studies of Hv1-mediated pH control in cells.

We chose 2-guanidinobenzimidazole-based (2GBI-based) Hv1 inhibitors (2GBI, Fig. 1A) as building block to synthesize light-sensitive molecules. The block of Hv1 relies on the guanidine and imidazole moieties of 2GBI that interact with amino-acid residues deeply located in the open channel pore [24, 25]; these 2GBI moieties, therefore, are not suitable for chemical modification. By contrast, the benzene moiety tolerates relatively large modifications without affecting the blocking efficiency [25]. Therefore, we covalently attached an azobenzene group to the 5(6)-position (tautomerization) of the benzimidazole core (Fig. 1B). We reasoned that the elongated *trans* form can reach the blocking site in

the channel pore, whereas the more bend *cis* form is either sterically hindered to reach the blocking site or blocks proton currents less efficiently (Fig. 1C). Synthesis started from commercially available 4-nitrobenzene-1,2-diamine (**1**), which was treated with dicyandiamide in refluxing HCl aq to yield 5(6)-nitro-2GBI (**2**) (Scheme 1). The guanidine moiety was protected as its bis-pivaloyl congener (**3**). Nitro reduction yielded aminobenzimidazole (**4**), from which all light-sensitive 2GBI derivatives (**photoGBI1-4**) were synthesized by sequential azo-coupling and deprotection (Scheme 1).

The electron-donating amino group at the 4'-position improves the photochemical properties in two respects. First, it red-shifts the absorption spectrum (λ_{max} > 450 nm); therefore, the photoswitch can be controlled by wavelengths that do not cause cell damage (450-500 nm). Second, the amino group speeds up the intrinsic *cis*-to-*trans* relaxation time [26, 27], which allows studying physiological processes on a sub-second timescale using a single light source. Furthermore, optimal compounds would be both water-soluble and membrane permeable, and combine a high blocking efficacy with a large light-dependent modulation. Such physicochemical properties can be tuned by substitutions at the 4'-amino group. However, because these properties cannot be predicted precisely, we synthetized and tested several analogs. In **photoGBI1**, we introduced an *N*,*N*-dimethylamino group at the 4'-position. In **photoGBI2**, one of the *N*-methyl groups was replaced by an *N*-hydroxyethyl group. To enhance water solubility, in **photoGBI3**, the *N*,*N*-dimethylamino group was replaced by an *N*-hydroxyethyl group, resulting in a secondary amine structure at the 4'-position. To promote membrane permeability, in **photoGBI4**, the *N*-hydroxyethyl group was replaced by the more lipophilic *N*-hydroxybutyl group. Compared to azobenzene, the UV-VIS spectra of the photoGBIs are red-shifted (λ_{max} ranging from 452 to 468 nm); the extinction coefficients ($\varepsilon_{\lambda max}$ ranging from 27,616 to 34,117 $M^{-1}cm^{-1}$) are characteristic for *N*-substituted 4'-aminobenzene-based photoswitches (Table S1 and Fig. S1).

We studied the pharmacological action of these compounds on a shorter, sperm-specific variant of human Hv1, called Hv1Sper. The variant activates more rapidly than Hv1 [28], facilitating pharmacological characterization. Proton currents were recorded in the voltage-clamp mode from excised inside-out membrane patches of *Xenopus laevis* frog oocytes. A voltage step from -60 mV to +80 mV activated Hv1Sper, giving rise to proton outward currents (black traces, Figs. 2A,B and S2A-D). When photoGBI1-4 solutions were bath applied, proton currents were strongly reduced (red traces; Fig. S2A-E, 20 μM photoGBI1-4, n = 4-6; Fig. 2B, 50 μM photoGBI4, n = 6). The effective block confirms that 2GBI-based inhibitors can be modified at the benzene group without drastic changes in blocking efficiency [25]. Photoisomerization diminished the proton-current blockage for all compounds, demonstrating a change in blocking efficiency by light. The light-dependent relative release of inhibition

was most pronounced for photoGBI2-4 (Fig. S2E,F). The kinetics of currents evoked by switching photoGBI3 and photoGBI4 was best fit with a double-exponential function, whereas kinetics evoked by switching compounds photoGBI1 and photoGBI2 was more complex (Fig. S2A-D). We focused on characterizing compounds photoGBI3 and photoGBI4. Both compounds rapidly release inhibition in response to light (Fig. S2C,D,G,H; 20 μM; photoGBI3, $\tau_{on\ fast}$ = 9 ± 4 ms, $\tau_{on\ slow}$ = 230 ± 150 ms, n = 6; photoGBI4, $\tau_{on\ fast}$ = 5 ± 3 ms, $\tau_{on\ slow}$ = 0.9 ± 0.5 s, n = 4). Due to fast thermal relaxation from *cis* to *trans*, the initial inhibition is rapidly restored in the dark (photoGBI3, $\tau_{off\ fast}$ = 23 ± 10 ms, $\tau_{off\ slow}$ = 190 ± 180 ms, n = 6; photoGBI4, $\tau_{off\ fast}$ = 17 ± 12 ms, $\tau_{off\ slow}$ = 0.7 ± 0.7 s, n = 4). Light-induced release of inhibition could be repeatedly induced without diminishing current amplitudes (Fig. S3A). Furthermore, the block was reversible: after wash out, proton currents returned to initial amplitudes (Fig. S3B). Excised patches from oocytes that did not express Hv1Sper did not show any proton currents and showed no response to light in the presence of any photoGBI (Fig. S3C).

We measured the inhibition of Hv1Sper currents at various concentrations of photoGBI4 in the dark and under light conditions (Fig. 2A-C). Light irradiation decreased the maximal inhibition from 89% to 57% and the IC_{50} increased from 9 to 13 μM (Fig. 2C). We next recorded an action spectrum of photoGBI4 (Fig. 2D). Irradiation with 430 nm light released the current block maximally. Compared to the absorption spectrum, the action spectrum was shifted by about 15 nm towards lower wavelengths. This difference might reflect a different dielectric environment, e.g. a lower polarity in the binding pocket compared to water. Polar solvents can shift the absorption spectrum of azobenzene (Fig. S4). Alternatively, photoisomerization might be more efficient for the first molecular electronic transition (”hidden” absorption peak at around 420 nm) than at the second transition (peak at 462 nm, Fig. S1).

Hv1 inhibitor 2GBI acts as open-channel blocker [24] that reaches the blocking site only in the open state of the channel. This blocking mechanism can be gleaned from electrophysiological recordings. Open-channel blockers, once bound, prevent channel closure and consequently slow down channel deactivation, a mechanism termed “foot-in-the-door” (Fig. S5A) [29]. In fact, photoGBI3 significantly increased the fast and slow deactivation time constants from 18 ± 5 to 28 ± 7 ms and from 100 ± 40 to 140 ± 30 ms, respectively (Fig. S5B,C; paired t-tests, p = 0.0001 and p = 0.02 for fast and slow components, n = 7). Another characteristic feature of open-channel blockers is a biphasic time course of channel activation, which becomes noticeable when channel activation is faster than the diffusion of the inhibitor to its blocking site. Hv1-F150A, a channel mutant with fast activation, shows biphasic activation kinetics in the presence of 2GBI [24]. Likewise, in the presence of photoGBI3, activation kinetics of Hv1-

F150A also becomes biphasic (Fig. S5D). In summary, like its parent compound 2GBI, photoGBI3 blocks Hv1 by an open-channel mechanism.

The blocking site of 2GBI is located at the intracellular side of Hv1, strongly suggesting that photoGBI switches are also intracellular blockers. The chemical congener Cl-GBI is membrane-permeable, which allows for convenient extracellular application [25]. To test membrane permeability, photoGBIs were applied to the extracellular side of the membrane during outside-out patch-clamp recordings (Fig. S6). Compounds photoGBI2 and photoGBI3 did not block currents when applied extracellularly; even after 5 min incubation time, only a minor modulation of the proton current occurred upon light stimulation of photoGBI2 (Fig. S6B,C). By contrast, photoGBI1 and photoGBI4 blocked the proton current upon extracellular application within a few minutes, indicating that substituents attached to the azobenzene core can render these compounds membrane-permeable (Fig. S6A,D).

Because of its membrane permeability and large photoswitch effect, we tested whether photoGBI4 blocks native proton currents in cells that express Hv1 or Hv1Sper. Macrophages express Hv1 and show sizeable proton currents ([30], Fig. 3A). Bath application of 100 μM photoGBI4 reduced the outward proton current of THP-1 macrophages by 42 ± 6% (Fig. 3A,B; n = 3). Light stimulation released this inhibition, leading to a reduced inhibition of 27 ± 6%. Human sperm express full-length Hv1 and a proteolytically cleaved variant Hv1Sper [28]. Bath application of 100 μM photoGBI4 reduced the outward proton current recorded from sperm by 55 ± 11% (Fig. 3C,D; n = 6), and light stimulation released this inhibition, leading to an inhibition of 24 ± 14%. Thus, photoGBI4 is suitable for photocontrolling native proton currents by blocking Hv1.

Here, we report on the synthesis and characterization of inhibitors, photoGBIs, that block proton flux through Hv1 channels in a light-dependent manner. The inhibitors contain an azobenzene moiety, mediating photoisomerization, a 2GBI moiety, mediating high-affinity block of Hv1 currents, and substituents at the azobenzene part that tune the inhibitor´s physicochemical and spectroscopic properties. In the dark, photoGBIs block Hv1 proton currents, whereas during irradiation with light, the block of Hv1 is released. PhotoGBIs have favorable features. The electron-donating amino group in the 4'-position of the azobenzene moiety results in a red-shifted absorption spectrum (400-460 nm) that is ideal for light stimulation in living cells. This strategy has been previously employed to obtain red-shifted switches for potassium channels and glutamate receptors [31, 7], avoiding UV damage and allowing for deeper penetration of biological tissue. The *cis* form of these photoswitches is thermally unstable and

rapidly relaxes to the *trans* conformation in the dark. Thus, a single wavelength is sufficient to control switching between conformations.

Several photoswitches that have been developed previously were covalently tethered to a target protein, either directly via a thiol-reactive group or remotely via a protein tag fused to the target protein [32, 33, 34]. These strategies are advantageous, because they provide specificity for the target protein. At the same time, tethered photoswitches require genetic engineering of the target protein, precluding application on natively expressed proteins. Non-tethered photoswitches like photoGBIs do not require genetic manipulation, making them applicable to a large range of organisms and cell types, including human sperm. PhotoGBIs freely diffuse and their target specificity is solely provided by high binding affinity of the blocking site. Due to its particular architecture, Hv1 might have a unique blocking site: Hv1 consists of only a voltage-sensor domain (VSD) and lacks the pore domain of "classical" voltage-gated ion channels. Thus, protons permeate Hv1 through the VSD, and the blocking site for 2GBI and its congeners is located within the VSD. Because no other native channel uses the VSD for ion permeation, this unusual ion pathway of Hv1 might inherently endow photoGBI with specificity for Hv1.

For further studies of Hv1-mediated proton flux, photoGBI4 seems to be the best choice. The block by photoGBI4 is strong and its modulation by light is fast and relatively large. Moreover, photoGBI4 is membrane permeable and can reach its intracellular blocking site even when applied from the outside. The photoswitches described here, in particular photoGBI4, should become useful tools to dissect the physiological role of Hv1 in pH-regulating pathways. For example, is Hv1 involved in the activation of the pH-sensitive CatSper Ca^{2+} channel in human sperm? How rapidly do changes in pH_i follow the block or unblock of Hv1? On a final note, the photoGBIs hold promise to control Hv1 activity not only temporally, but also locally in different cellular compartments. Thereby, photoGBIs might allow studying rapid propagation of pH changes inside cells.

METHODS

Additional methods can be found in the Supporting Information.

Synthesis

Synthesis and spectra for all compounds can be found in the Supporting Information.

DNA constructs and expression in Xenopus oocytes

DNA constructs were cloned and sequenced using standard techniques. Hv1Sper and Hv1-F150A encoded on the pGEMHE vector for expression in oocytes was linearized with Nhe1 and transcribed using the T7 mMessage mMachine kit (Ambion, Austin, TX). *Xenopus laevis* oocytes were purchased from EcoCyte (Castrop-Rauxel, Germany), generously donated by C. Volk (Bonn Rhein-Sieg University), or harvested from our own frog colony. Housing and surgical procedures on *Xenopus* frogs were performed according to the district veterinary office and the German law of animal protection (license 84-02.04.2016.A077). Oocytes were kept at 12 °C in ND96, containing (in mM): NaCl 96, Na-pyruvate 2.5, KCl 2, $CaCl_2$ 1.8, $MgCl_2$ 1, 2-(4-(2-hydroxyethyl)-1-piperazinyl)-ethanesulfonic acid (HEPES) 5, and gentamicin 100 mg/l, titrated to pH = 7.5 with NaOH). One to three days prior to patch-clamp recordings, oocytes were injected with 50.6 nl of RNA encoding Hv1Sper or Hv1-F150A. Immediately before the experiment, the cells were manually devitellinated.

Electrophysiology

Patch pipettes were pulled from borosilicate capillaries (Hilgenberg, Malsfeld, Germany) using a DMZ puller (Zeitz Instruments GmbH, Martinsried, Germany) and fire polished with a Narishige MF-830 microforge (Narishige, Tokyo, Japan). Proton currents from Hv1 expressed in oocytes were recorded from excised patches in the inside-out or outside-out configuration at RT using an Axopatch 200B amplifier (Molecular Devices, Union City, CA). The initial resistance of the pipettes used for these recordings was 0.9-3.5 MΩ. Data were acquired with a Digidata 1440A acquisition board (Molecular Devices) connected to a PC running ClampEx (Molecular Devices). Light was applied through an inverted IX71 microscope (Olympus, Tokyo, Japan) equipped with a 60x oil immersion objective (Olympus Apo N, NA 1.49). The action spectrum (Fig. 2D) was recorded using a monochromator (Photon Technology International, Bensheim, Germany) equipped with a xenon lamp and set to a spectral bandwidth of 20 nm. All other recordings were performed using a Spectra X (Lumencor, Beaverton, OR) or a M450LP1 LED (Thorlabs, Newton, NJ) as a light source. Photoswitchable inhibitors were diluted in the recording solution from a 50 mM stock in dimethyl sulfoxide (DMSO) before bath application. Light intensities were measured with a PS19Q sensor connected to a FieldMax-TOP power meter for visible light (Coherent, Dieburg, Germany) at the level of the recording stage. For excised patch-clamp recordings, the bath and pipette solution contained (in mM): 2-(*N*-morpholino)ethanesulfonic acid (MES) 100 (pH 6) or HEPES 100 (pH 7), methane sulfonic acid (MS) 40, tetraethylammonium chloride (TEA-Cl) 5, and ethylene glycol-bis-(2-aminoethylether)-*N*,*N*,*N'*,*N'*-tetraacetic acid (EGTA) 5. The pH was adjusted to 6 or 7 with TEA hydroxide (TEA-OH); the osmolarity was 190 - 220 mOsm. Human semen samples were donated by

healthy adult males with their prior written consent and the approval of the ethic committee of the University of Bonn (042/17). The sperm cells were purified by a 'swim up' procedure (Strünker *et al.*, 2011) in artificial human tubular fluid (HTF) containing (in mM): NaCl 93.8, Na-lactate 21.4, HEPES 21, KCl 4.69 , $NaHCO_3$ 4, glucose 2.78 , $CaCl_2$ 2.04, Na-pyruvate 0.33, $MgSO_4$ 0.2, and KH_2PO_4 0.37, adjusted to pH 7.35 with NaOH at 37°C. Subsequently, human serum albumin (3 mg/ml) was added to the purified sperm sample. For patch-clamp recordings, several microliters of a $1*10^7$ sperm cells/ml sample were pipetted onto a poly-*L*-lysine-coated (PLL) 5 mm cover slip immersed in a HEPES saline-based buffer (HS) containing (in mM): NaCl 130, *D*-mannitol 15, KCl 5, $CaCl_2$ 2, $MgSO_4$ 1, and HEPES 20; pH was adjusted to 7.4 with NaOH). Sperm were allowed to settle and adhere to the coated glass for 5 minutes and were observed under an IX71 inverted microscope equipped with a 60x water immersion objective (Olympus UPlanSApo). Only sperm that showed flagellar beating and that had their head stuck to the cover slip were used for recordings. After sealing, the bath solution was exchanged to the recording solution containing (in mM): *N*-Methyl-*D*-glucamine 120, MES 100, TEA-Cl 5, and EGTA 2, titrated to pH 6 with MS. The intracellular pipette solution was the same as the bath solution. THP-1 cells were pipetted into the bath chamber and allowed to settle for 10 min in physiological extracellular solution containing (in mM): NaCl 140, KCl 6, $MgCl_2$ 1, $CaCl_2$ 1.5, glucose 5.5, and HEPES 20, adjusted to pH 7.4 with NaOH. Currents from THP-1 cells were recorded with the same intracellular pipette solution as sperm cells, and with a bath solution containing (in mM): *N*-Methyl-*D*-glucamine 120, HEPES 100, TEA-Cl 5, EGTA 1, adjusted to pH 7 with MS. Relative inhibition (Fig. 2C, 3B,D, S2E, S6E) was calculated as the ratio between the steady-state outward current after and before inhibitor application. Relative release of inhibition (Fig. S2F) was calculated as the difference between the relative inhibition in the dark minus the relative inhibition during light. The change in proton current (ΔI, Fig. 2D) was calculated as the difference between the outward current with and without light. Kinetics of the photoswitch response (Fig. S2C,D) and the tail current (Fig. S5B) was fitted with a double-exponential function ($I(t) = I_{slow} \cdot e^{-\frac{t}{\tau_{slow}}} + I_{fast} \cdot e^{-\frac{t}{\tau_{fast}}}$). Two-tailed paired t-tests were performed with Igor Pro (Wavemetrics, Portland, OR). Throughout the manuscript, we report mean ± SD.

UV-VIS spectra

Baseline-corrected spectra of the respective compounds (20 µM concentration) were obtained in a solution containing (in mM): HEPES 100, MS 40, TEA-Cl 5, and EGTA 5, adjusted to pH 7 with TEA-OH, on

a Varian Cary 5000 (Agilent, Santa Clara, CA). Extinction coefficients were calculated according to Lambert-Beer.

ASSOCIATED CONTENT

Supporting Information

The Supporting Information is available free of charge on the ACS Publication website at DOI:

Supporting Figures 1-6, photoGBI synthesis and ^{1}H and ^{13}C NMR spectra.

AUTHOR INFORMATION

Corresponding author

*E-mail: thomas.berger@caesar.de

ORCID

Thomas K. Berger: 0000-0001-9358-1315

Notes

The authors declare no competing financial interest.

ACKOWLEDGMENTS

Financial support for this work was provided by the German-Israeli Foundation (GIF) Young Scientist Program to TKB (G-2405-418.13/2015) and the Deutsche Forschungsgemeinschaft (DFG) to TKB (BE5506/3-1). We thank Luis Alvarez for his careful help with light sources.

References

[1] Szobota, S. and Isacoff, E. Y. (2010) Optical control of neuronal activity. *Annu. Rev. Biophys. 39*, 329–348.

[2] Kramer, R., Mourot, A., and Adesnik, H. (2013) Optogenetic pharmacology for control of native neuronal signaling proteins. *Nat. Neurosci. 16*, 816–823.

[3] Broichhagen, J., Frank, J. A., and Trauner, D. (2015) A roadmap to success in photopharmacology. *Acc. Chem. Res. 48*, 1947–1960.

[4] Banghart, M., Borges, K., Isacoff, E., Trauner, D., and Kramer, R. H. (2004) Light-activated ion channels for remote control of neuronal firing. *Nat. Neurosci. 7*, 1381–1386.

[5] Volgraf, M., Gorostiza, P., Numano, R., Kramer, R. H., Isacoff, E. Y., and Trauner, D. (2006) Allosteric control of an ionotropic glutamate receptor with an optical switch. *Nat. Chem. Biol. 2*, 47–52.

[6] Mourot, A., Fehrentz, T., Le Feuvre, Y., Smith, C. M., Herold, C., Dalkara, D., Nagy, F., Trauner, D., and Kramer, R. H. (2012) Rapid optical control of nociception with an ion-channel photoswitch. *Nat. Methods 9*, 396–402.

[7] Kienzler, M. A., Reiner, A., Trautman, E., Yoo, S., Trauner, D., and Isacoff, E. Y. (2013) A red-shifted, fast-relaxing azobenzene photoswitch for visible light control of an ionotropic glutamate receptor. *J. Am. Chem. Soc. 135*, 17683–17686.

[8] Reiner, A. and Isacoff, E. Y. (2014) Tethered ligands reveal glutamate receptor desensitization depends on subunit occupancy. *Nat. Chem. Biol. 10*, 273–280.

[9] Lemoine, D., Habermacher, C., Martz, A., Méry, P., Bouquier, N., Diverchy, F., Taly, A., Rassendren, F., Specht, A., and Grutter, T. (2013) Optical control of an ion channel gate. *Proc. Natl. Acad. Sci. U. S. A. 110*, 20813–20818.

[10] Schönberger, M., Althaus, M., Fronius, M., Clauss, W., and Trauner, D. (2014) Controlling epithelial sodium channels with light using photoswitchable amilorides. *Nat. Chem. 6*, 712–719.

[11] Levitz, J., Pantoja, C., Gaub, B., Janovjak, H., Reiner, A., Hoagland, A., Schoppik, D., Kane, B., Stawski, P., Schier, A. F., Trauner, D., and Isacoff, E. Y. (2013) Optical control of metabotropic glutamate receptors. *Nat. Neurosci. 16*, 507–516.

[12] Broichhagen, J., Jurastow, I., Iwan, K., Kummer, W., and Trauner, D. (2014) Optical control of acetylcholinesterase with a tacrine switch. *Angew. Chem. Int. Edit. 53*, 7657–7660.

[13] Frank, J. A., Yushchenko, D. A., Hodson, D. J., Lipstein, N., Nagpal, J., Rutter, G. A., Rhee, J.-S., Gottschalk, A., Brose, N., Schultz, C., and Trauner, D. (2016) Photoswitchable diacylglycerols enable optical control of protein kinase C. *Nat. Chem. Biol. 12*, 755–762.

[14] Rovira, X., Trapero, A., Pittolo, S., Zussy, C., Faucherre, A., Jopling, C., Giraldo, J., Pin, J., Gorostiza, P., Goudet, C., and Llebaria, A. (2016) OptoGluNAM4.1, a photoswitchable allosteric antagonist for real-time control of mGlu4 receptor activity. *Cell Chem. Biol. 23*, 929–934.

[15] Ramsey, I. S., Ruchti, E., Kaczmarek, J. S., and Clapham, D. E. (2009) Hv1 proton channels are required for high-level NADPH oxidase-dependent superoxide production during the phagocyte respiratory burst. *Proc. Natl. Acad. Sci. U. S. A. 106*, 7642–7647.

[16] El Chemaly, A., Okochi, Y., Sasaki, M., Arnaudeau, S., Okamura, Y., and Demaurex, N. (2010) VSOP/Hv1 proton channels sustain calcium entry, neutrophil migration, and superoxide production by limiting cell depolarization and acidification. *J. Exp. Med. 207*, 129–139.

[17] Wu, L.-J., Wu, G., Akhavan Sharif, M. R., Baker, A., Jia, Y., Fahey, F. H., Luo, H. R., Feener, E. P., and Clapham, D. E. (2012) The voltage-gated proton channel Hv1 enhances brain damage from ischemic stroke. *Nat. Neurosci. 15*, 565–573.

[18] Capasso, M., Bhamrah, M. K., Henley, T., Boyd, R. S., Langlais, C., Cain, K., Dinsdale, D., Pulford, K., Khan, M., Musset, B., Cherny, V. V., Morgan, D., Gascoyne, R. D., Vigorito, E., DeCoursey, T. E.,

MacLennan, I. C. M., and Dyer, M. J. S. (2010) HVCN1 modulates BCR signal strength via regulation of BCR-dependent generation of reactive oxygen species. *Nat. Immunol. 11*, 265–272.

[19] Iovannisci, D., Illek, B., and Fischer, H. (2010) Function of the HVCN1 proton channel in airway epithelia and a naturally occurring mutation, M91T. *J. Gen. Physiol. 136*, 35–46.

[20] Wang, Y., Li, S. J., Wu, X., Che, Y., and Li, Q. (2012) Clinicopathological and biological significance of human voltage-gated proton channel Hv1 protein overexpression in breast cancer. *J. Biol. Chem. 287*, 13877–13888.

[21] Wang, Y., Wu, X., Li, Q., Zhang, S., and Li, S. J. (2013) Human voltage-gated proton channel Hv1: a new potential biomarker for diagnosis and prognosis of colorectal cancer. *PLoS One 8*, e70550.

[22] Lishko, P. V., Botchkina, I. L., Fedorenko, A., and Kirichok, Y. (2010) Acid extrusion from human spermatozoa is mediated by flagellar voltage-gated proton channel. *Cell 140*, 327–337.

[23] Florman, H. M., Jungnickel, M. K., and Sutton, K. A. (2010) Shedding light on sperm pHertility. *Cell 140*, 310–312.

[24] Hong, L., Pathak, M. M., Kim, I. H., Ta, D., and Tombola, F. (2013) Voltage-sensing domain of voltage-gated proton channel Hv1 shares mechanism of block with pore domains. *Neuron 77*, 274–287.

[25] Hong, L., Kim, I. H., and Tombola, F. (2014) Molecular determinants of Hv1 proton channel inhibition by guanidine derivatives. *Proc. Natl. Acad. Sci. U. S. A. 111*, 9971–9976.

[26] Bandara, H. M. D. and Burdette, S. C. (2012) Photoisomerization in different classes of azobenzene. *Chem. Soc. Rev. 41*, 1809–1825.

[27] Sadovski, O., Beharry, A. A., Zhang, F., and Woolley, G. A. (2009) Spectral tuning of azobenzene photoswitches for biological applications. *Angew. Chem. Int. Edit. 48*, 1484–1486.

[28] Berger, T. K., Fußhöller, D. M., Goodwin, N., Bönigk, W., Müller, A., Dokani Khesroshahi, N., Brenker, C., Wachten, D., Krause, E., Kaupp, U. B., and Strünker, T. (2017) Post-translational cleavage of Hv1 in human sperm tunes pH- and voltage-dependent gating. *J. Physiol. (Lond.) 595*, 1533–1546.

[29] Yeh, J. Z. and Armstrong, C. M. (1978) Immobilisation of gating charge by a substance that simulates inactivation. *Nature 273*, 387–389.

[30] DeCoursey, T. E. and Cherny, V. V. (1996) Voltage-activated proton currents in human THP-1 monocytes. *J. Membr. Biol. 152*, 131–140.

[31] Mourot, A., Kienzler, M. A., Banghart, M. R., Fehrentz, T., Huber, F. M. E., Stein, M., Kramer, R. H., and Trauner, D. (2011) Tuning photochromic ion channel blockers. *ACS Chem. Neurosci. 2*, 536–543.

[32] Broichhagen, J. and Trauner, D. (2014) The in vivo chemistry of photoswitched tethered ligands. *Curr. Opin. Chem. Biol. 21*, 121–127.

[33] Broichhagen, J., Damijonaitis, A., Levitz, J., Sokol, K. R., Leippe, P., Konrad, D., Isacoff, E. Y., and Trauner, D. (2015) Orthogonal optical control of a g protein-coupled receptor with a snap-tethered photochromic ligand. *ACS Cent. Sci. 1*, 383–393.

[34] Berlin, S. and Isacoff, E. (2017) Synapses in the spotlight with synthetic optogenetics. *EMBO Reports 18*, 677–692.

Figure 1. Strategy for photocontrolling Hv1. A. 2-guanidinobenzimidazole (2GBI), an intracellular open channel blocker of Hv1. **B.** Structure of photoswitchable 2GBI-derivates, containing an azobenzene moiety coupled to 2GBI. Arrows indicate switching from *trans* (top, red) to *cis* conformation (bottom, blue) by light and the reversal reaction by thermal relaxation. **C.** Cartoon showing block of Hv1 without light (*trans* conformation) and release of block with light (*cis* conformation).

Scheme 1. Synthesis of 2GBI-based photoswitches (photoGBI). Conditions: **a)** Dicyandiamide, HCl, H_2O, reflux. **b)** Piv_2O, py, 80 °C. **c**) $NH_4(HCOO)$, Pd/C, MeOH, RT. **d)** 1. HCl aq, $NaNO_2$, H_2O/EtOH, 0 °C, 2. *N*-alkylanilines, 0 °C to RT. **e)** 1 M NaOH aq, MeOH 60 °C.

Figure 2. Characterization of photoGBI4. A. Structure of photoGBI4. **B.** Excised inside-out patch-clamp recording from a frog oocyte expressing Hv1Sper. Hv1Sper current elicited by a depolarizing voltage step before (black) and after (red) bath application of 50 µM photoGBI4 under symmetric pH conditions ($pH_i = pH_o = 7$). Blue bar indicates light stimulation (438 and 475 nm, ~23.7 mW/mm²) **C.** Dose-response curve of photoGBI4 determined in the dark (black) and under light stimulation (blue; 438 and 475 nm, ~23.7 mW/mm²). Data points were fitted with the Hill equation. Dark: IC_{50} = 9 ± 1 µM, h = 2.5 ± 0.7, max = 0.89 ± 0.04; light: IC_{50} = 13 ± 1 µM, h = 2.4 ± 0.5, max = 0.57 ± 0.03 (n = 3-7). **D.** Action spectrum (normalized ΔI) and normalized absorption of photoGBI4 (10 µM). The change in Hv1Sper current (ΔI, inset) during a depolarizing voltage step from -60 to +80 mV upon light stimulation was determined for wavelengths between 400-570 nm (n = 3). Error bars represent SD.

Figure 3. Light-induced release from proton current inhibition by photoGBI4 in macrophages and sperm. A. Whole-cell recording of proton currents from a THP1 macrophage elicited by a depolarizing voltage step before (black) and after (red) bath application of 100 µM photoGBI4. Blue bar indicates light stimulation (450 nm, ~23 mW/mm^2). **B.** Relative inhibition of proton currents in THP1 macrophages by 100 µM photoGBI4 is significantly reduced under light stimulation (paired t-test, p = 0.007, n = 3). **C.** Whole-cell recording of proton currents from a human sperm cell elicited by a depolarizing voltage step before (black) and after (red) bath application of 100 µM photoGBI4. Blue bar indicates light stimulation (438 and 475 nm, ~23.7 mW/mm^2). **D.** Relative inhibition of proton currents in human sperm by 100 µM photoGBI4 is significantly reduced under light stimulation (paired t-test, p = $1x10^{-5}$, n = 6).

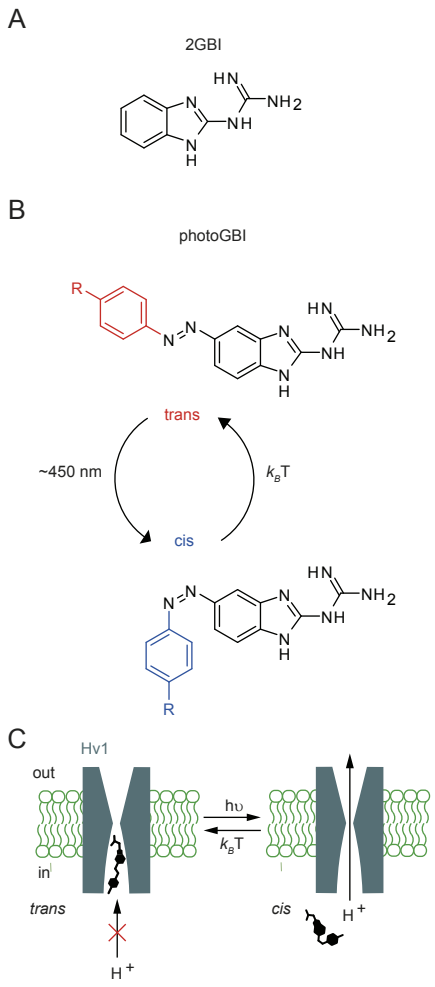
A
2GBI
B
photoGBI
trans
~450 nm
k_BT
cis
C
Hv1
out
in
hυ
k_BT
trans
cis
H^+
H^+

Figure 1

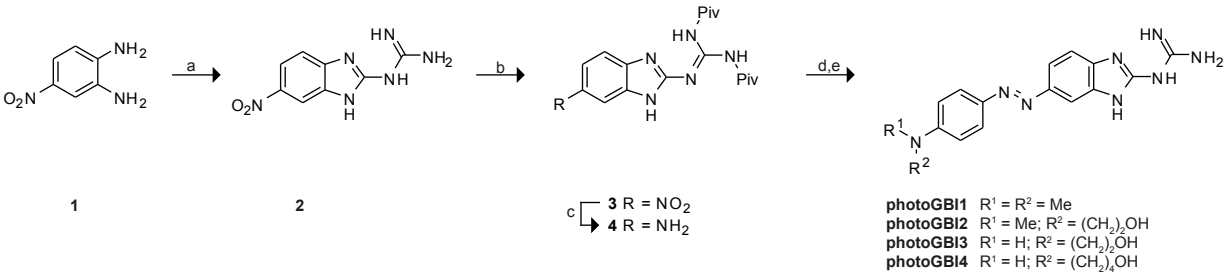
a
b
c
d,e
1
2
3 R = NO2
4 R = NH2
photoGBI1 R1 = R2 = Me
photoGBI2 R1 = Me; R2 = (CH2)2OH
photoGBI3 R1 = H; R2 = (CH2)2OH
photoGBI4 R1 = H; R2 = (CH2)4OH

Scheme 1

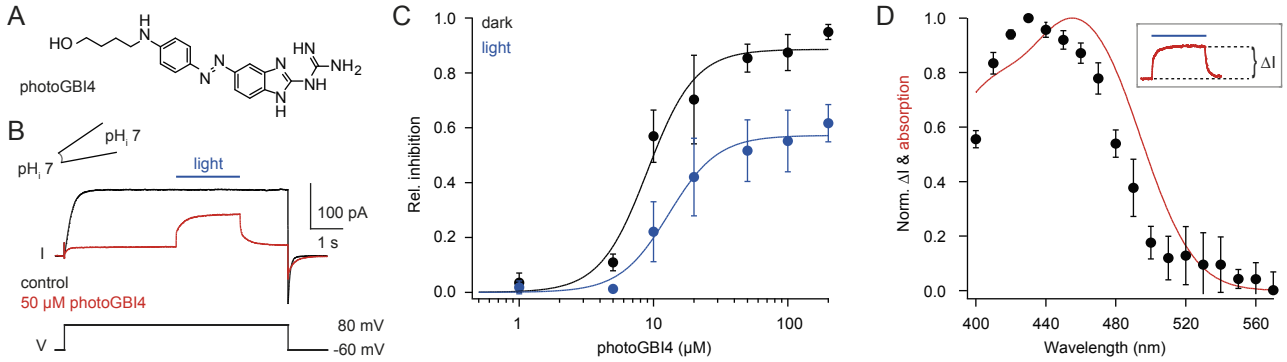
A
HO
H
N
N
N
HN
NH2
NH
N
H
photoGBI4
B
pHi 7
pHi 7
light
100 pA
1 s
I
control
50 µM photoGBI4
V
80 mV
-60 mV
C
dark
light
Rel. inhibition
1.0
0.8
0.6
0.4
0.2
0.0
1
10
100
photoGBI4 (µM)
D
Norm. ΔI & absorption
ΔI
400
440
480
520
560
Wavelength (nm)

Figure 2

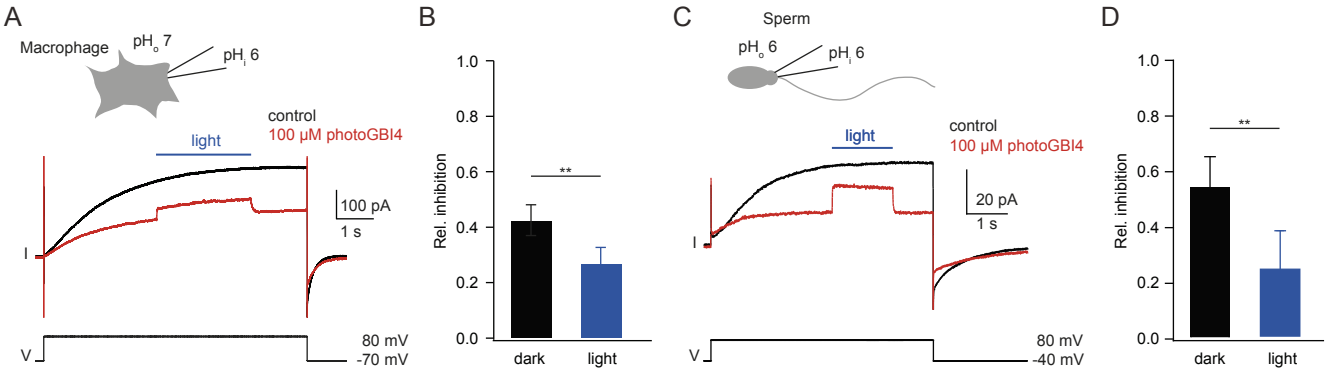
A
Macrophage
pH$_o$ 7
pH$_i$ 6
light
control
100 μM photoGBI4
100 pA
1 s
I
V
80 mV
-70 mV
B
Rel. inhibition
1.0
0.8
0.6
0.4
0.2
0.0
**
dark
light
C
Sperm
pH$_o$ 6
pH$_i$ 6
light
control
100 μM photoGBI4
20 pA
1 s
I
V
80 mV
-40 mV
D
Rel. inhibition
1.0
0.8
0.6
0.4
0.2
0.0
**
dark
light

Figure 3